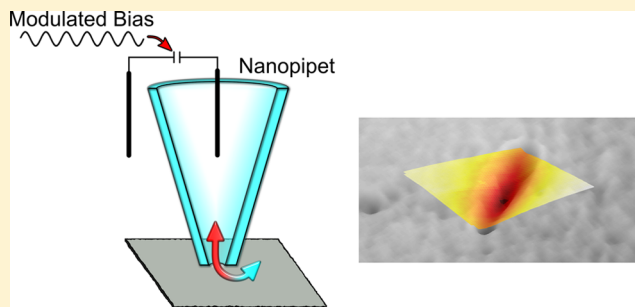


Bias Modulated Scanning Ion Conductance Microscopy

Kim McKelvey,[†] David Perry,^{†,‡} Joshua C. Byers,[†] Alex W. Colburn,[†] and Patrick R. Unwin^{*,†}[†]Department of Chemistry and [‡]MOAC Doctoral Training Centre, University of Warwick, Coventry, CV4 7AL, United Kingdom

S Supporting Information

ABSTRACT: Nanopipets are versatile tools for nanoscience, particularly when used in scanning ion conductance microscopy (SICM) to determine, in a noncontact manner, the topography of a sample. We present a new method, applying an oscillating bias between a quasi-reference counter electrode (QRCE) in the SICM nanopipet probe and a second QRCE in the bulk solution, to generate a feedback signal to control the distance between the end of a nanopipet and a surface. Both the amplitude and phase of the oscillating ion current, induced by the oscillating bias and extracted using a phase-sensitive detector, are shown to be sensitive to the probe–surface distance and are used to provide stable feedback signals. The phase signal is particularly sensitive at high frequencies of the oscillating bias (up to 30 kHz herein). This development eliminates the need to physically oscillate the probe to generate an oscillating ion current feedback signal, as needed for conventional SICM modes. Moreover, bias modulation allows a feedback signal to be generated without any net ion current flow, ensuring that any polarization of the quasi reference counter electrodes, electro-osmotic effects, and perturbations of the supporting electrolyte composition are minimized. Both feedback signals, magnitude and phase, are analyzed through approach curve measurements to different surfaces at a range of distinct frequencies and via impedance measurements at different distances from a surface. The bias modulated response is readily understood via a simple equivalent circuit model. Bias modulated (BM)-SICM is compared to conventional SICM imaging through measurements of substrates with distinct topographical features and yields equivalent results. Finally, BM-SICM with both amplitude and phase feedback is used for topographical imaging of subtle etch features in a calcite crystal surface. The 2 modes yield similar results, but phase-detection opens up the prospect of faster imaging.



Scanning ion conductance microscopy (SICM) is a versatile, solution phase technique that uses a nanopipet immersed in, and filled with, an electrolyte solution to interrogate the properties of a sample surface, most commonly the topography.^{1–3} An ion current flows through the end of the nanopipet by applying a bias between a quasi-reference counter electrode (QRCE) in the nanopipet and another QRCE in the bulk of the solution, as illustrated in Figure 1. The ion current depends primarily on the solution resistance in the nanopipet and, critically, the solution resistance in the gap between the end of the nanopipet and the sample surface.^{2,3} As a nanopipet approaches a surface (typically, when the probe–surface distance is less than the nanopipet diameter),⁴ the gap resistance increases, which leads to a drop in the ion current. Importantly, this change in current means that the nanopipet detects the surface without ever making physical contact, so that SICM is a rather powerful noncontact imaging technique.² SICM has thus proven particularly effective for mapping the local topography of very delicate samples such as living cells,^{3,5–7} by using constant distance,^{8–11} the hopping/backstep/standing approach,^{5,12–14} or hybrid¹⁵ modes to move the nanopipet over the sample. SICM has also been used to investigate ion flow through nanopores^{11,16} and as a tool for mapping the mechanical properties of live cells.^{17,18}

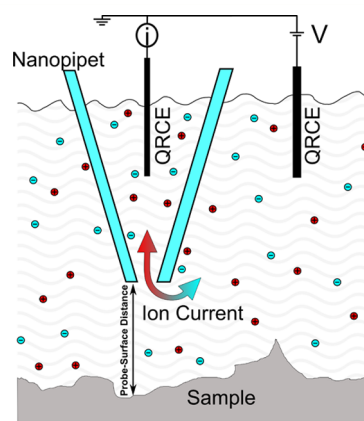


Figure 1. The SICM configuration, with one QRCE in the nanopipet and another in the bulk of the solution. A bias (V) is applied to the bulk QRCE and the ion current (i) is measured at the QRCE in the nanopipet. The ion current depends on the probe–surface distance. In BM-SICM, an oscillating bias (V) is applied between the two QRCEs.

Received: January 23, 2014

Accepted: March 11, 2014

Published: March 11, 2014

The initial implementations of SICM used the direct ion current between the QRCEs as a feedback signal to regulate the nanopipet–sample distance.¹ Typically, the surface was detected by the probe when the ion current value dropped by 0.2–3% from the bulk ion current.¹⁰ However, the ion current is susceptible to changes in the bulk solution resistance (e.g., due to thermal fluctuations), partial blockages of the nanopipet, and changes in the polarized QRCEs, all of which can cause the ion current to change, reducing the stability of the feedback response.

A distance-modulated approach was introduced to improve the stability of the feedback response and is now commonly used.^{2,3,6,9,19–23} The distance between the nanopipet and the surface is modulated which induces an alternating component of the ion current (AC), in addition to the direct ion current, when the tip is close to the surface. There is usually an increase in the magnitude of the alternating ion current with decreasing nanopipet–surface separation.^{19,20} The AC is detected with a lock-in amplifier at the same frequency as the driving oscillation, reducing noise and improving the sensitivity of the surface detection. However, the need to physically oscillate the probe can induce convective fluid movement around the tip and also reduces the response time of the feedback signal (as it is now limited by the oscillation frequency of the probe).

An alternative method, pulse mode SICM,^{24,25} applies a current pulse between the QRCEs, and the change in potential needed to drive this pulse is measured. As mentioned above, as the probe approaches a surface, the resistance generally increases and therefore the potential needed to drive the current pulse increases. Thus, the probe is first moved a small increment toward a surface; a current pulse is generated, and the potential is measured. Depending on the signal, the probe is moved another increment toward the surface until a desired (potential) set point is reached, when the probe position is measured.²⁴ In this way, a topographical map of the surface can be built up pixel by pixel, although the process is rather lengthy and the approach has not been widely adopted.

Herein, we explore an alternative mechanism to generate a feedback response in SICM, via bias modulation (BM). An oscillating bias is applied between the QRCEs, eliminating the need to physically oscillate the probe, and a phase-sensitive detector (a lock-in amplifier) is used to extract the amplitude and phase of the oscillating ion current. We show that this produces a stable feedback parameter (amplitude or phase) for SICM over a wide range of frequencies (from 200 Hz to 30 kHz herein). We explore the frequency dependent response using impedance measurements at different distances from a surface. Oscillating the bias between the QRCEs about 0 V ensures that there is no net ion current flow, in contrast to all other implementations of SICM. This ensures that any polarization of the QRCEs and perturbation of the supporting electrolyte concentration in and around the probe are minimized and that fluid movement induced by electro-osmotic effects through the end of the nanopipet is minimized. We note that preliminary limited measurements of this type were reported recently but were of a low resolution, at limited frequencies, and neglected to use any phase-sensitive detection of the AC ion current.²⁶ We demonstrate the use of this feedback mechanism for topographical imaging by mapping well-defined structures, including gold bands on glass and subtle etch features on a calcite crystal surface using both the magnitude and the phase of the AC response as feedback

parameters. These examples serve to highlight the future prospects for the use of this new mode of SICM.

METHODS

Solutions. Milli-Q reagent grade water (resistivity of ca. 18.2 M Ω cm at 25 °C) was used for all solutions. 100 mM KCl (Sigma-Aldrich) was typically used as an electrolyte solution for the SICM measurements, except for experiments to explore supporting electrolyte concentration effects, where the concentration was varied in the range of 0.01–100 mM. For the studies of calcite, a 10 mM CaCl₂ (Sigma-Aldrich) solution was used. A 3 mM maleic acid (Sigma-Aldrich) solution was used to etch the calcite surface before imaging.²⁷

Nanopipets. 60 nm radius nanopipets were fabricated from borosilicate glass pipets (o.d. 1.2 mm, i.d. 0.69 mm, Harvard Apparatus) using a laser puller (P-2000, Sutter Instruments; pulling parameters: Line 1: Heat 350, Fil 3, Vel 30, Del 220, Pul _; Line 2: Heat 350, Fil 3, Vel 40, Del 180, Pul 120). Each nanopipet used was filled with the same electrolyte solution as employed for the bulk solution and an Ag/AgCl QRCE was inserted. The nanopipet was then mounted on a piezoelectric positioner (see below) and placed in solution close to the sample. A second Ag/AgCl QRCE was placed in the bulk of the solution.

Substrates. Glass bottomed Petri dishes (3512, WillcoWells), gold band structures on glass (fabricated using the lift off lithography method to produce 700 nm high and 50 μ m wide gold features), and calcite (Iceland Spar, Richard Tayler Minerals, Surrey, UK; cleaved and etched for 5 min in 3 mM maleic acid solution that was constantly stirred, resulting in the formation of etch pits) were used as substrates.

Instrumentation. As described previously,²⁸ a 38 μ m piezoelectric positioner (P-753-3CD, Physik Intrumente) was used for movement of the nanopipet normal to the sample (Figure 1). The sample was moved laterally under the tip with a two axis piezoelectric positioner system (Nano-BioS300, Mad City Laboratories Inc.). A bias (V) was applied directly to the QRCE in the bulk of solution, and the current was measured at the QRCE in the nanopipet using a custom wideband current-to-voltage converter (DC –300 kHz (–3 dB)). A lock-in amplifier (SR830, Stanford Research Systems) was used to generate an oscillating bias that was applied directly to the bulk QRCE. Some conventional distance-modulated SICM measurements⁹ were also made, for comparison, and in this case, the bias voltage was added to the control signal for the 38 μ m piezoelectric positioner so as to modulate the nanopipet position normal to the sample. The lock-in amplifier was used to detect the oscillating components (the magnitude and phase) of the ion current. The instrument was controlled, and data collected, through a FPGA card (7852R, National Instruments) that was programmed using LabVIEW (2013, National Instruments). Impedance measurements were made using a Gamry Femtostat (FAS2-38039), with spectra acquired using Gamry Framework Data Acquisition Software (6.04).

Bias Modulated SICM Procedure. An oscillating bias (10 mV rms amplitude), with a frequency between 200 Hz and 30 kHz, was applied. For the initial approach and for the approach curve measurements, the nanopipet was moved toward the surface at a rate of 100 nm s^{–1} until the surface was detected as a change in either the magnitude or the phase of the oscillating component of the ion current (vide infra).

Maps and line traces of the local topography of substrates of interest were generated in a hopping mode, where a series of

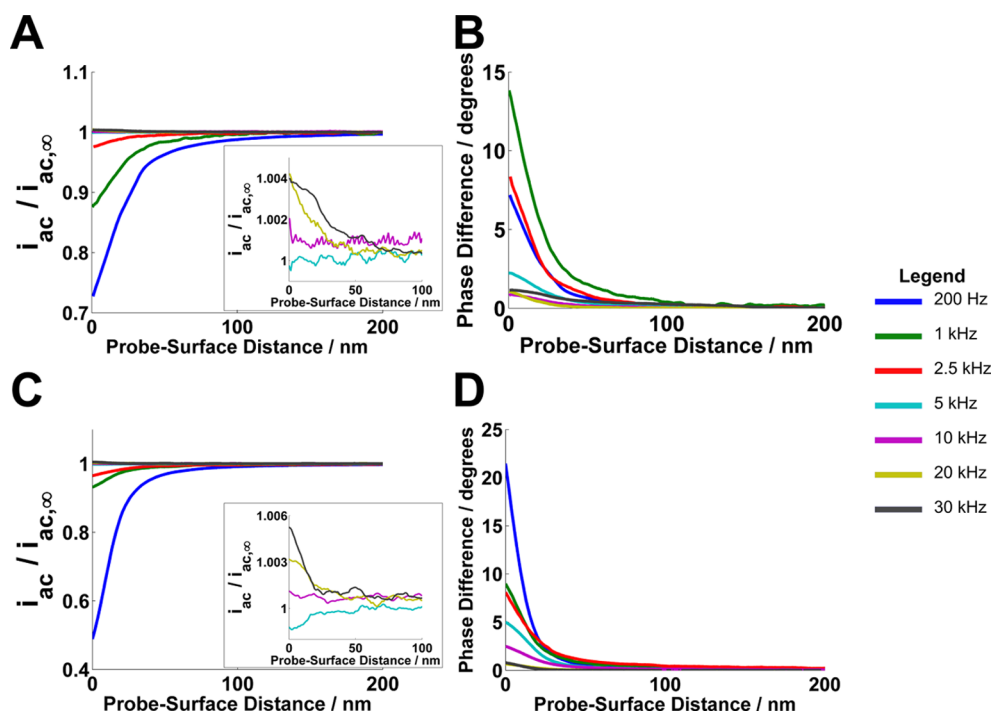


Figure 2. Approach curves, each with a separate pipet (60 nm radius, 10 mV rms bias oscillation in 100 mM KCl) to an insulating glass surface and a nonbiased conducting gold surface over a range of frequencies. (A) Normalized magnitude of the oscillating ion current over a glass surface. (B) Phase difference magnitude compared to the bulk of the oscillating ion current over a glass surface. (C) Normalized magnitude of the oscillating ion current over an unbiased gold surface. (D) Phase difference magnitude compared to the bulk of the oscillating ion current over an unbiased gold surface.

nanopipet approaches were made at different lateral positions (in a defined grid pattern) over the surface. At each position, the nanopipet was approached to the surface at a speed of $1 \mu\text{m s}^{-1}$ until the surface was detected as the amplitude or phase reaching a desired user defined set point. The nanopipet was then retracted $1 \mu\text{m}$ and then moved laterally to a new position where the process was repeated. The position of the piezoelectric positioners when the desired set point was attained was used to generate the maps (and line traces) of the local topography.

Distance Modulated SICM. The tip was oscillated normal to the surface using the oscillating potential generated by the lock-in amplifier, at a frequency of 230 Hz with 10 nm peak-to-peak amplitude. The QRCE in the bulk solution was biased at 0.3 V. Maps of the local topography were generated in a hopping mode, as described above, except that the oscillating ion current was generated through the oscillating motion of the probe normal to the surface.⁹

Impedance Measurements. A nanopipet was positioned close to a glass surface, and a Gamry Femtostat was connected to the QRCEs. The probe was moved in steps toward the surface, and at each step, an impedance measurement (between 1 Hz and 100 kHz with 9 points per decade and 10 mV rms) was taken. Before each impedance measurement, the potential was allowed to equilibrate for 10 s, and a series of measurements at each step took ca. 90 s. Equivalent circuit models were fitted using a simplex method with 300 iterations using Gamry Echem Analyst software.

RESULTS AND DISCUSSION

Approach Curves. Nanopipets (60 nm in radius) were approached at a velocity of 100 nm s^{-1} in 100 mM KCl to both

an insulating glass bottomed Petri dish and an unbiased conducting gold surface. The electrolyte concentration ensured that the ion current through the nanopipet showed ohmic behavior without any rectification phenomena.²⁹ Note that the absolute nanopipet–surface distance was estimated from the point of inflection in the amplitude and phase response, which we assign to the nanopipet making physical contact with the surface. Thus, each approach curve was made with a separate tip. Typical BM-SICM approach curves at a range of frequencies are presented in Figure 2.

In the bulk, far from the surface, the magnitude and phase of the oscillating ion current were constant at stable finite values. The absolute values of each depended on the bias modulation frequency as described in the Impedance Measurements section below (and shown as the bulk data in Figure 4A–C). These values were maintained until the nanopipet approached within (approximately) a tip diameter (or less) of the surface, when the magnitude and phase of the oscillating ion current changed (as shown in Figure 2), with both the insulating and unbiased conducting surfaces showing a fairly similar response. At low frequencies, the amplitude drops with probe–surface distance, but this effect was diminished with increasing frequency until, at frequencies above 10 kHz, the amplitude actually increased very slightly with the decrease in probe–surface distance (see insets in Figure 2A,C). The phase difference magnitude always increased with a decrease in probe–surface distance, although the extent of the increase depends on the frequency and at close distances to some extent the substrate. Importantly, these data show that modulating the bias enables the surface to be sensed readily through changes in the oscillation ion current magnitude and phase, making this an attractive feedback signal for SICM imaging.

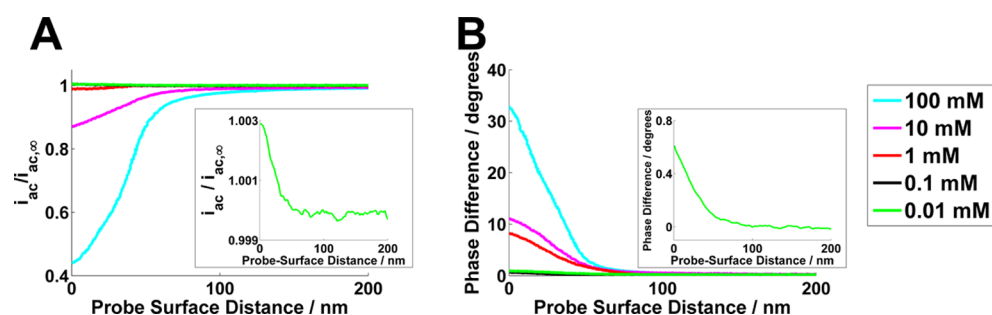


Figure 3. Approach curves (for a 60 nm radius pipet with a 10 mV rms bias oscillation at 200 Hz) to an insulating glass surface in a range of supporting electrolyte (KCl) concentrations. (A) Normalized magnitude of the oscillating current. (B) Phase difference magnitude compared to the bulk of the oscillating current.

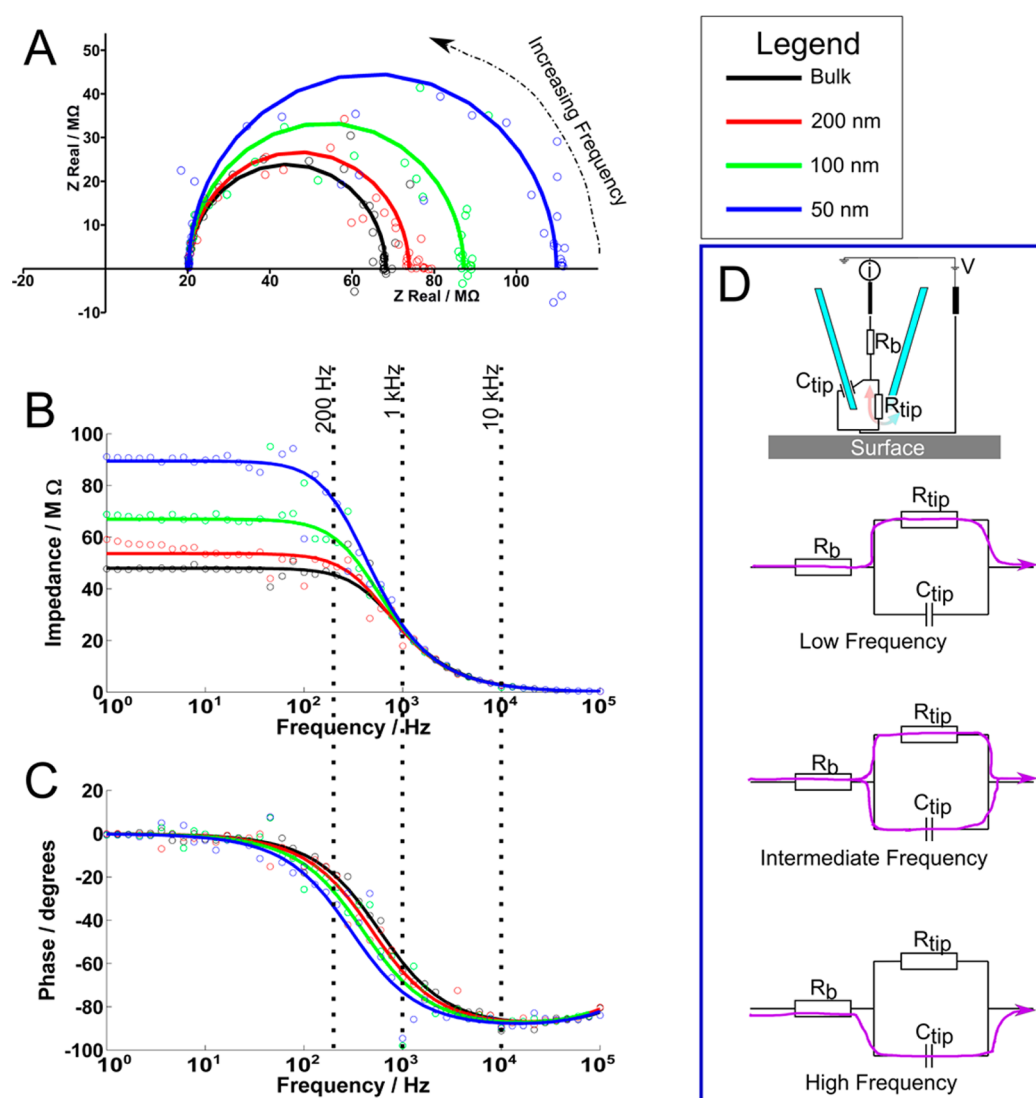


Figure 4. (A) Nyquist plot showing the impedance in bulk, at 200, 100, and 50 nm from a glass surface for a 60 nm radius nanopipet in 100 mM KCl. (B) Impedance magnitude at the different probe–surface distances as a function of frequency. (C) Phase as a function of frequency. In each case, the points are data and the solid lines are a fit to a simple equivalent circuit. (D) Schematic of the equivalent electrical circuit (a parallel RC component in series with a resistor), with the current flow paths at low, intermediate, and high frequencies, where R_b is the bulk resistance of the solution, R_{tip} is the resistance in the end of the pipet and in the probe–surface gap, and C_{tip} is the capacitance across the glass walls of the nanopipet.

While SICM usually employs relatively high electrolyte concentrations,² which is thus the main focus of the paper, we also explored the effect of electrolyte concentration. The approach curve response was found to depend on the

supporting electrolyte concentration, as shown in Figure 3A,B. These data are for a fixed oscillation frequency of 200 Hz to a glass substrate in various concentrations of KCl in the range of 100 to 0.01 mM. In general, as the supporting

electrolyte concentration decreases, there is a smaller amplitude and phase response as the probe approaches the surface. At low (0.1 mM and below) electrolyte concentrations, as shown in the insets in Figure 3A,B, the amplitude of the oscillation actually increases very slightly (by just 0.3%) with a decrease in the nanopipet–surface distance, while the phase difference magnitude continues to increase as the probe approaches the surface, although by just 0.5°. These data highlight the sensitivity with which BM-SICM measurements can be made and that a wide range of electrolyte concentrations should be employable. The impedance measurements and model that follow provide some rationalization of the approach curve data. Moreover, as we show below, these responses can be explained and predicted using a simple physical model.

Impedance Measurements. To further explore the response of BM-SICM, we carried out impedance measurements (in 100 mM KCl) with a nanopipet at different distances from a surface. Experiments were carried out at an insulating glass surface, which presented a smoother surface. The probe was moved in increments toward the surface, and at each height, an impedance measurement was made. The probe was held stationary for 90 s during the impedance measurement; however, in principle, thermal drift could change the probe–surface distance during this time.³⁰ We estimate from repeat approaches and measurements of a nanopipet to a surface that thermal drift would be no more than a maximum of 15 nm over this time period (see Supporting Information Figure S1), a distance that should not significantly influence the main features of our results. The low degree of thermal drift is consistent with other SICM measurements we have recently reported.²⁸

Impedance measurements in bulk solution and at distances of approximately 200, 100, and 50 nm from a glass surface are shown as a Nyquist plot in Figure 4A. The impedance data create a hemispherical curve in the upper right quadrant of the complex plane, with the low frequency data points on the real axis and the hemispherical curve traced out as the frequency increases. This response is typical for a nanopipet in a bulk solution with high electrolyte concentrations and no bias offset.³¹ As the nanopipet nears the surface, the low frequency response moves to the right, corresponding to an increase in resistance, as would be expected on the basis of conventional SICM.^{1,4,10} However, the general shape of the impedance curves is maintained.

The impedance data can also be represented as a function of frequency in the format of a Bode plot, as shown in Figure 4B,C, which allows the range of frequencies over which the main changes in the amplitude or phase occur to be identified. At frequencies below ca. 100 Hz, there is a clear and pronounced change in the amplitude response with probe–surface distance (decrease in amplitude with decreasing distance as discussed above), but this becomes attenuated at the higher frequencies. Above 500 Hz, the changes are predominantly confined to the phase response. In fact, a window for observing changes in the phase with frequency at finite distances from the surface is apparent between ca. 10 Hz and 20 kHz. The upper limit opens up the possibility of fast imaging in the future.

The approach curves, shown in Figure 2A,B, were carried out at constant frequency, and the positions of the 200 Hz, 1 kHz, and 10 kHz values are indicated in Figure 4B,C. For a frequency of 200 Hz, both the frequency and phase of the approach curves change with distance. At a frequency of 1 kHz,

the phase change is significant while the change in amplitude is severely attenuated. With a frequency of 10 kHz, there is no significant change in amplitude with probe–surface separation, but the change in the phase with distance is still detectable.

The impedance response in 100 mM KCl can be described by a simple equivalent electrical circuit, a parallel RC component in series with a second resistor as is shown in Figure 4D. The bulk resistance of the solution (both inside and outside the nanopipet) is described by the resistor, R_b , while the end of the tip (including the tip–surface gap) is described, in simplest terms, by a resistor and capacitor in parallel (R_{tip} and C_{tip}), where R_{tip} represents the resistance at the end of the tip (including the tip–surface gap) and C_{tip} represents the capacitance across the glass walls of the nanopipet. Although the RC component at the end of the probe could be broken down into multiple subcomponents, this is the simplest representation that effectively captures the nature of the response, as evident from the close agreement between experiment and the model. The values of the components of the simple equivalent electrical circuit were determined by fitting the simple model to the impedance data and are shown in Table 1. Note that this model describes the nanopipet

Table 1. Parameters Used to Fit the Impedance Data in Figure 4A–C, Using the Model in Figure 4D

distance	R_b/Ω	R_{tip}/Ω	C_{tip}/F
bulk	3.5×10^4	4.8×10^7	5.7×10^{-12}
200 nm	4.0×10^4	5.4×10^7	6.0×10^{-12}
100 nm	4.2×10^4	6.7×10^7	6.0×10^{-12}
50 nm	3.6×10^4	8.9×10^7	5.9×10^{-12}

response in high electrolyte solution, which is most commonly used. In low electrolyte solutions, ion current rectification due to inadequate screening of the charge on the walls of the nanopipet (and surface) becomes apparent, and this influences the impedance response.³¹

The resistance in the end of the tip (and tip–substrate gap), R_{tip} , is much larger than the resistance in the rest of the solution, as for conventional SICM.² As the nanopipet approaches the surface, R_{tip} increases, as also expected for conventional SICM.² The capacitance stays fairly constant (ca. 6 pF) with the change of probe–surface distance.

At low frequencies (below ca. 100 Hz), the current flows predominantly through the resistor of the parallel RC component, as shown schematically in Figure 4D. At intermediate frequencies (between ca. 100 and 500 Hz), the current flows through both the resistor R_{tip} and capacitor C_{tip} , while at high frequencies (above ca. 500 Hz) the current flows predominantly through the capacitor, as is also shown schematically in Figure 4D. Only the resistance, R_{tip} , changes significantly with the probe–surface distance, and therefore, the frequency dependent response can easily be understood using the equivalent circuit model.

Using the well-known expression for the resistance between the end of a nanopipet and surface,² the simple equivalent model can further be used to predict the approach curves for high electrolyte solution. The tip resistance is equivalent to the access resistance plus the bulk resistance.

$$R_{tip} = R_{bulk} + \frac{\frac{3}{2} \log \frac{r_o}{r_i}}{\kappa \cdot \pi \cdot d}$$

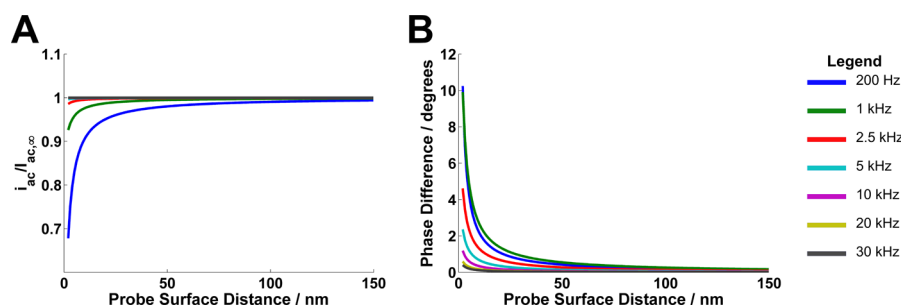


Figure 5. Theoretical approach curves (see text for details) for a 60 nm radius nanopipet in 100 mM KCl at a range of BM frequencies. (A) The normalized magnitude of the oscillating current. (B) The phase difference magnitude of the oscillating current.

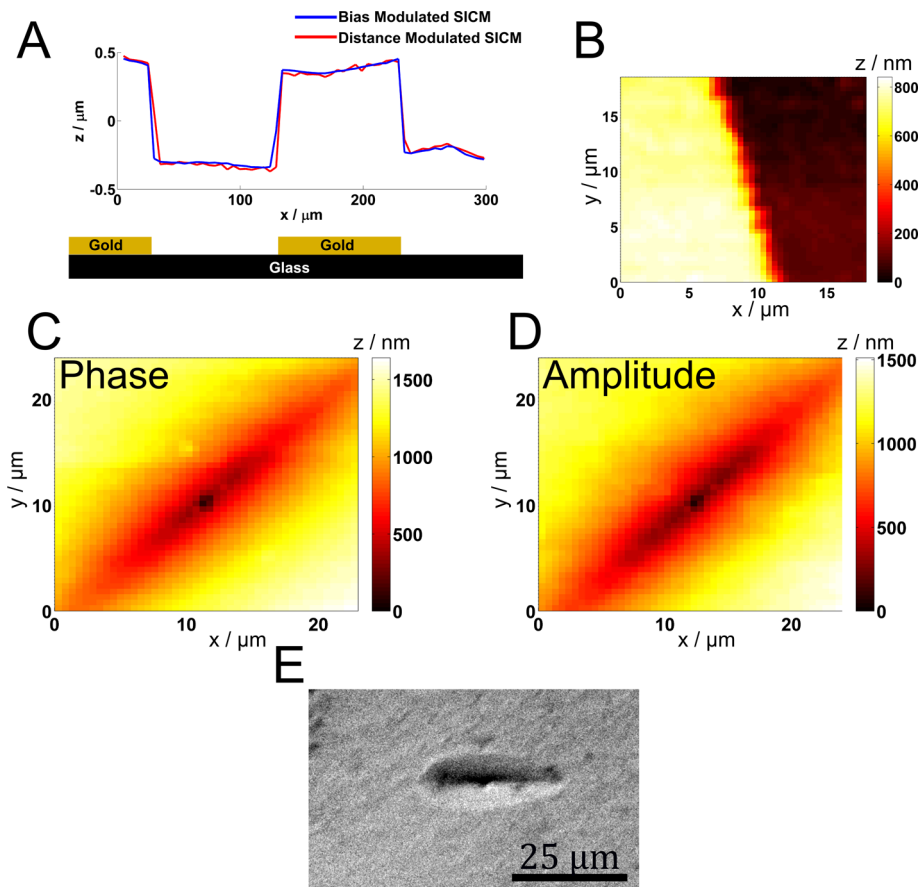


Figure 6. (A) Line scan across glass surface with gold bands in both conventional distance-modulated SICM and BM-SICM. (B) Topography map of the edge of a gold band feature on glass imaged using BM-SICM at 1 kHz using phase as the feedback with a set point of 1° . (C) Topography of a calcite etch pit determined using BM-SICM at 1 kHz using phase as the feedback with a set point of 1° . (D) Topography of the same calcite etch pit determined using BM-SICM at 1 kHz using the AC amplitude as feedback with a set point of 0.995. (E) Optical image of a typical calcite etch pit for comparison with the SICM data.

where r_o and r_i are the outer and inner tip radii, κ is the solution conductivity, d is the tip–substrate separation distance, and R_{bulk} is the fitted tip resistance in bulk solution (see Table 1), where the effects of the surface are not detectable. This expression was substituted into the equivalent circuit model, and the predicted approach curves at a range of frequencies are shown in Figure 5. These curves are a reasonable approximation to the data presented in Figure 2A,B.

For future implementations, it could be advantageous to increase the frequency at which a significant surface response is observed, as this would reduce the time constant of the feedback response and therefore allow the nanopipet to be moved at a greater lateral speed over a surface. This can be

achieved by decreasing the resistance in our simple model, which can be achieved experimentally by increasing the concentration of the supporting electrolyte and/or by changing the shape (for instance the cone angle) or size of the nanopipet. The resolution of SICM is governed by the size of the nanopipet, with smaller nanopipets providing higher resolution images. Herein, we have considered 60 nm radius nanopipets. However, different sized nanopipets will continue to exhibit a bias modulated response, with the magnitude and frequency range of the response scaling with the nanopipet size. On the basis of our impedance model, smaller nanopipets (which have a higher resistance) should show a response at lower frequencies. In addition, smaller nanopipets can exhibit an

ion current rectification response that will also affect the magnitude of the response (in fact, the 60 nm nanopipets used in lower electrolyte concentrations, as shown in Figure 3, exhibited an ion current rectification response and provided a bias modulated response on approach to a surface). Interestingly, at frequencies above 10 kHz, we observe a very small increase in the amplitude of the oscillating current as the probe approaches the surface (as is shown in the insets in Figure 2A,C). These responses are not captured in our impedance data as the probe was not placed closer than 50 nm from the surface and so is not captured in our simple equivalent circuit model above. We also observed a similar small increase in the amplitude at close distances, at a lower frequency (200 Hz), at low electrolyte concentrations (Figure 3A). This suggests the current flow between the nanopipet and bulk interacts with the diffuse double layer that forms at the glass substrate surface, where there is both a higher ion concentration and where there may also be consequentially an ion current rectification phenomena between the end of the nanopipet and the surface.³² This is an interesting observation and one that BM-SICM could play a significant role in elucidating in the future.

Mapping Topography. Initially, we compared the topography generated by distance-modulated SICM,^{19,20} the predominant SICM technique, to that of BM-SICM using an amplitude set point of 0.983. Figure 6A shows line profiles of the topography of a sample with unbiased gold features (conducting) on a glass (insulating) surface that was imaged with both modes in 100 mM KCl. An oscillating frequency of 200 Hz was used for both the bias and distance modulation. The line profiles are practically identical for the two techniques, confirming that BM-SICM produces the same topography as distance-modulated SICM but without the need to physically oscillate the nanopipet or generate a net ion current. These data confirm that BM-SICM is not affected by the nature of the substrate when the tip images at or about a radius from the surface (i.e., has a small set point) are consistent with the approach curve data presented herein. A topographical map of a gold band edge is shown in Figure 6B generated using BM-SICM (with a bias oscillation of 1 kHz and 10 mV rms) and using the alternative phase signal for feedback with set point 1°. The image shows a sharp, straight edge at the gold–glass interface and a height of 700 nm as expected.

Finally, we imaged etch pits in calcite using BM-SICM with both amplitude and phase set points. The etch pits were formed by dissolving the calcite in maleic acid for 5 min, which creates distinct oval shaped pits in the surface. The dissolution was stopped by removing the maleic acid solution and replacing it with 10 mM CaCl₂, in which the SICM mapping was conducted. Etch pits in calcite are oval depressions in the surface, as shown in the optical image in Figure 6E. The local topography was imaged in BM-SICM (with a bias oscillation of 1 kHz and 10 mV rms) in a hopping mode (1 μ m separation between hops) with a 60 nm nanopipet. The topography of a single etch pit is shown in Figure 6 using the phase signal, with set point 1° (C), and AC amplitude, with set point 0.995 (D), as feedback parameters, respectively. The etch pit is clearly resolved and corresponds to typical etch pits as observed by optical microscopy (E). This demonstrates that BM-SICM can be used to determine the topography of interesting practical samples. In the future, the capability of BM-SICM to be carried out at higher frequencies should allow dynamic surfaces to be followed with good time resolution.

CONCLUSIONS

Modulating the bias between the QRCEs in SICM allows the probe–surface distance to be detected through the amplitude and phase components of the oscillation ion current, detected with a lock-in amplifier. This provides a simple, stable method to detect the probe–substrate distance that does not require the physical movement of a probe or the application of a net ion current. This reduces both convective and electro-osmotic fluid movement, detrimental effects from extensive polarization of the QRCEs, and changes of the supporting electrolyte composition within the nanopipet that can be problematic with conventional SICM.

The frequency dependence of the probe–surface distance response can be readily understood using a simple equivalent circuit model that we developed for an inert surface and was elucidated through impedance measurements at different probe–surface distances. This has allowed us to identify a window in which either the magnitude (up to ca. 500 Hz) or phase (between ca. 100 Hz and 30 kHz) of the oscillation ion current can be used to sense the probe–surface distance. Interestingly, at very close pipet–surface distances (at frequencies above 10 kHz in 100 mM KCl or at lower frequencies in lower supporting electrolyte concentrations), there is a subtle effect of the surface which is likely due to the nanopipet ion flow interacting with the diffuse double layer at the surface. The sensitivity of this technique in detecting these subtle responses indicates that BM-SICM not only is a topographical tool but also could prove to be a powerful method for investigating other properties of surfaces and interfaces.

To illustrate the capability of BM-SICM for imaging, we have measured substrate topography, the dominant use of SICM. The topography obtained using BM-SICM (in a hopping mode) was equivalent to that generated by conventional distance-modulated SICM over both insulating and nonbiased conducting substrates, confirming the validity of the technique. An interesting sample of an etched calcite surface was imaged using both the amplitude and phase of the oscillating ion current as feedback parameters. In both cases, similar images were obtained and the topography of an individual subtle etch pit in the surface was easily identified. These data provide a platform for the future use of BM-SICM for imaging surface processes and dynamics.

ASSOCIATED CONTENT

Supporting Information

Additional information, as noted in text, on the thermal drift present in the system. This material is available free of charge via the Internet at <http://pubs.acs.org>.

AUTHOR INFORMATION

Corresponding Author

*E-mail: P.R.Unwin@warwick.ac.uk.

Notes

The authors declare no competing financial interest.

ACKNOWLEDGMENTS

We thank the European Research Council (ERC-2009-AdG247143-QUANTIF) and the EPSRC (though the MOAC DTC) for funding. The research leading to these results has received funding from the European Union Seventh Framework Programme (FP7/2007-2013) under grant agree-

ment No. 329953. We thank Dr. Aleix G. Güell for the preparation of the gold/glass surfaces.

■ REFERENCES

- (1) Hansma, P. K.; Drake, B.; Marti, O.; Gould, S. A. C.; Prater, C. B. *Science* **1989**, *243*, 641–643.
- (2) Chen, C.; Zhou, Y.; Baker, L. A. *Ann. Rev. Anal. Chem.* **2012**, *5*, 207–228.
- (3) Happel, P.; Thatenhorst, D.; Dietzel, I. D. *Sensors* **2012**, *12*, 14983–15008.
- (4) Edwards, M. A.; Williams, C. G.; Whitworth, A. L.; Unwin, P. R. *Anal. Chem.* **2009**, *81*, 4482–4492.
- (5) Yang, X.; Liu, X.; Zhang, X.; Lu, H.; Zhang, J.; Zhang, Y. *Ultramicroscopy* **2011**, *111*, 1417–1422.
- (6) Ushiki, T.; Nakajima, M.; Choi, M.; Cho, S.-J.; Iwata, F. *Micron* **2012**, *43*, 1390–1398.
- (7) Klenerman, D.; Korchev, Y. E.; Davis, S. J. *Curr. Opin. Chem. Biol.* **2011**, *15*, 1–8.
- (8) Shevchuk, A. I.; Frolenkov, G. I.; Sánchez, D.; James, P. S.; Freedman, N.; Lab, M. J.; Jones, R.; Klenerman, D.; Korchev, Y. E. *Angew. Chem., Int. Ed.* **2006**, *45*, 2212–2216.
- (9) Shevchuk, A. I.; Gorelik, J.; Harding, S. E.; Lab, M. J.; Klenerman, D.; Korchev, Y. E. *Biophys. J.* **2001**, *81*, 1759–1764.
- (10) Korchev, Y. E.; Bashford, C. L.; Milovanovic, M.; Vodyanoy, I.; Lab, M. J. *Biophys. J.* **1997**, *73*, 653–658.
- (11) Chen, C.-C.; Derylo, M. A.; Baker, L. A. *Anal. Chem.* **2009**, *81*, 4742–4751.
- (12) Novak, P.; Li, C.; Shevchuk, A. I.; Stepanyan, R.; Caldwell, M.; Hughes, S.; Smart, T. G.; Gorelik, J.; Ostanin, V. P.; Lab, M. J.; Moss, G. W. J.; Frolenkov, G. I.; Klenerman, D.; Korchev, Y. E. *Nat. Methods* **2009**, *6*, 279–281.
- (13) Happel, P.; Dietzel, I. D. *J. Nanobiotechnol.* **2009**, *7*, 7.
- (14) Takahashi, Y.; Murakami, Y.; Nagamine, K.; Shiku, H.; Aoyagi, S.; Yasukawa, T.; Kanzaki, M.; Matsue, T. *Phys. Chem. Chem. Phys.* **2010**, *12*, 10012–10017.
- (15) Zhukov, A.; Richards, O.; Ostanin, V.; Korchev, Y.; Klenerman, D. *Ultramicroscopy* **2012**, *121*, 1–7.
- (16) Chen, C.-C.; Zhou, Y.; Baker, L. A. *ACS Nano* **2011**, *5*, 8404–8411.
- (17) Schäffer, T. E. *Anal. Chem.* **2013**, *85*, 6988–6994.
- (18) Rheinlaender, J.; Schäffer, T. E. *Soft Matter* **2013**, *9*, 3230–3236.
- (19) Li, C.; Johnson, N.; Ostanin, V.; Shevchuk, A.; Ying, L.; Korchev, Y.; Klenerman, D. *Prog. Nat. Sci.* **2008**, *18*, 671–677.
- (20) Pastré, D.; Iwamoto, H.; Liu, J.; Szabo, G.; Shao, Z. *Ultramicroscopy* **2001**, *90*, 13–9.
- (21) Rheinlaender, J.; Geisse, N. A.; Proksch, R.; Schäffer, T. E. *Langmuir* **2011**, *27*, 697–704.
- (22) Chen, C.; Baker, L. A. *Analyst* **2011**, *136*, 90–97.
- (23) Zhou, Y.; Chen, C.-C.; Baker, L. A. *Anal. Chem.* **2012**, *84*, 3003–3009.
- (24) Mann, S. A.; Hoffmann, G.; Hengstenberg, A.; Schuhmann, W.; Dietzel, I. D. *J. Neurosci. Methods* **2002**, *116*, 113–117.
- (25) Happel, P.; Hoffmann, G.; Mann, S. A.; Dietzel, I. D. *J. Microsc.* **2003**, *212*, 144–151.
- (26) Kawashima, T.; Matsugase, T.; Tanaka, K.; Nagai, M.; Shibata, T.; Mineta, T.; Makino, E. *Microelectron. Eng.* **2012**, *98*, 663–667.
- (27) Compton, R. G.; Pritchard, K. L.; Unwin, P. R.; Grigg, G.; Silvester, P.; Lees, M.; House, W. A. *J. Chem. Soc. Faraday Trans. 1* **1989**, *85*, 4335–4366.
- (28) Nadappuram, B. P.; McKelvey, K.; Al Botros, R.; Colburn, A. W.; Unwin, P. R. *Anal. Chem.* **2013**, *85*, 8070–8074.
- (29) Wei, C.; Bard, A. J.; Feldberg, S. W. *Anal. Chem.* **1997**, *69*, 4627–4633.
- (30) Kim, J.; Shen, M.; Nioradze, N.; Amemiya, S. *Anal. Chem.* **2012**, *84*, 3489–3492.
- (31) Feng, J.; Liu, J.; Wu, B.; Wang, G. *Anal. Chem.* **2010**, *82*, 4520–4528.
- (32) Sa, N.; Lan, W.; Shi, W.; Baker, L. A. *ACS Nano* **2013**, *7*, 11272–11282.